The Institute of Space and Astronautical Science
Report No. 646, June 1992

Effect of the Flow Non-uniformity on the Mixing Layer at the Interface of Parallel Supersonic Flows

By

Takashi ABE[*1] and Katsushi FUNABIKI,[*2]
Hironobu ARIGA,[*3]
and Katsumi HIRAOKA[*4]

(April 30, 1992)

The effect of flow non-uniformity on the supersonic mixing layer was investigated. The mixing layer is formed at the interface between the parallel supersonic flows of air and helium. The mixing layer was directly investigated by measuring the concentration ratio of helium. As for the flow non-uniformity, the stream-wise pressure gradient and the shock wave penetrating the mixing layer were considered. The effect of the stream-wise pressure gradient enhances the mixing rate by around 2 times in comparison with the one of the mixing layer without the effect. The shock impingement further enhances the mixing rate in comparison with the one of the mixing layer with the stream-wise pressure gradient but without the shock impingement. The enhancement of the mixing layer growth rate caused by the flow non-uniformities is attributed to the vorticity enhancement at the mixing layer, for which the baroclinic torque is a strong candidate.

1. INTRODUCTION

The mixing process in the supersonic flow attracts much attention in a various field of research such as a scramjet engine [*1*]. Extensive studies by not only experimental method [*2, 3, 4*] but also theoretical and numerical method [*5*] were concentrated on this field. Among them, Papamoschou and Roshko [*3*] examined the compressibility effect on the mixing layer at the interface of the parallel supersonic flows and clarified the fact that the growth rate of the mixing layer is reduced by the compressibility effect in comparison with the

[*1]Associate professor, Institute of Space and Astronautical Science, Yoshinodai 3-1-1, Sagamihara, Kanagawa 229, Japan. Member AIAA.
[*2]Research assistant, Institute of Space and Astronautical Science.
[*3]Graduate student, Musashi Institute of Technology.
[*4]Associate professor, School of Engineering, Tokai University. Member AIAA.

one without compressibility effect. In their study, the mixing process was examined by means of the flow visualization technique by Schlieren photography. Recently several workers concentrate their attention to enhancing the growth rate of the supersonic mixing layer. [*4, 5*] This is because the enhancement of mixing implies the improvement of the performance of scramjet engine for example. In the present paper, we attempt to clarify the effect of the flow no-uniformity on the growth rate of the mixing layer formed at the interface of the parallel supersonic flows. For this purpose the structure of mixing layer was examined by the in-site measurement of the concentration ratio of the gas mixture. As for the flow no-uniformity, we consider the stream-wise pressure gradient and the shock wave impinging on the mixing layer.

2. Experimental Facility

To examine the effect of stream-wise pressure gradient on the mixing layer, we employed the wedge nozzle (Case 2) to attain the supersonic flow having the stream-wise pressure gradient, and the shock free nozzle (Case 1) for comparison to attain the uniform supersonic flow. To examine the effect of shock impingement on the mixing layer, a shock generator is mounted on the Case 2 configuration. We designate this as Case 3. Two nozzles are combined to produce the parallel supersonic flows as shown in Fig. 1. Both nozzles are two-dimensional ones and their transverse width is 100 mm. Separate two-dimensional supersonic flows are generated through each nozzle and the mixing layer is generated at the interface of the supersonic flows. In Case 2, we must note that slight non-uniformity along the vertical direction cannot be avoided as a cost of the stream-wise pressure gradient. In Case 3, the shock generator having a step of 3 mm height, produces a shock wave impinging on the mixing layer while it produces expansion wave as well as shock wave.

The present experimental facility is depicted in Fig. 2. Supersonic flow is attained by supplying a high pressure gas in a short time. For the lower nozzle, a pressurized helium gas with room temperature is employed while, for the upper nozzle, is employed the high enthalpy air which is produced at the stagnant region generated behind the reflected shock wave driven by the shock tube. That is, as far as the upper nozzle is concerned, the supersonic flow is generated in a manner of the shock tunnel. The reason for using the shock tunnel is a future extension of the experiment. The shock tube is driven by using fast-action-valves instead of the conventional rapture disks. The fast-action-valve just behind the nozzle for air can be replaced by a conventional rapture disk if necessary. The helium flow is initiated by opening the fast-action-valve just behind the nozzle for helium. These fast-action-valves enable us to operate the facility in good reproducibility. The details of the experimental facility can be referred to Ref. 6.

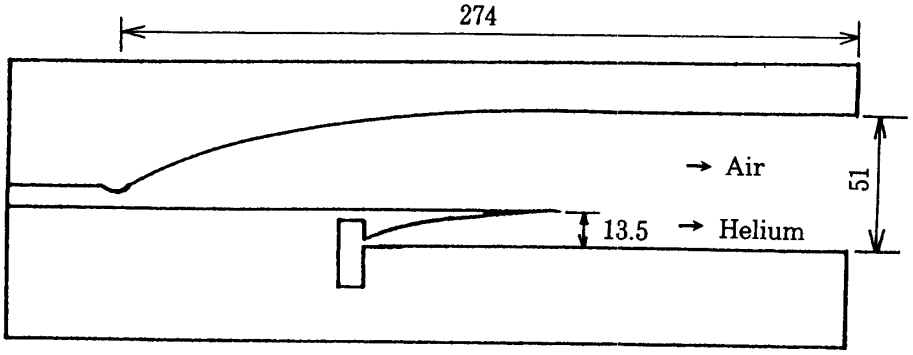

(a) Case 1

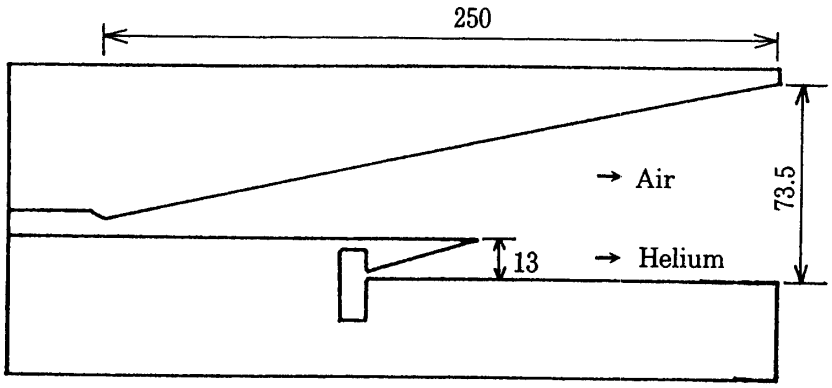

(b) Case 2

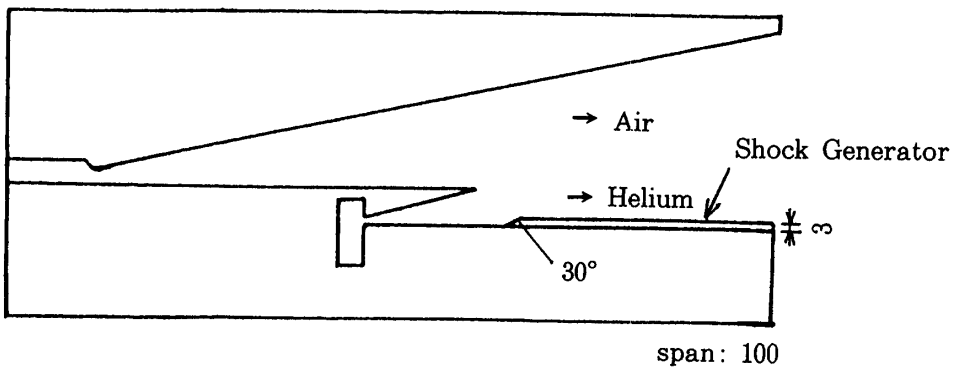

(c) Case 3

Fig. 1. Nozzle configurations of Case 1 (in (a)), Case 2 (in (b)) and Case 3 (in (c)).

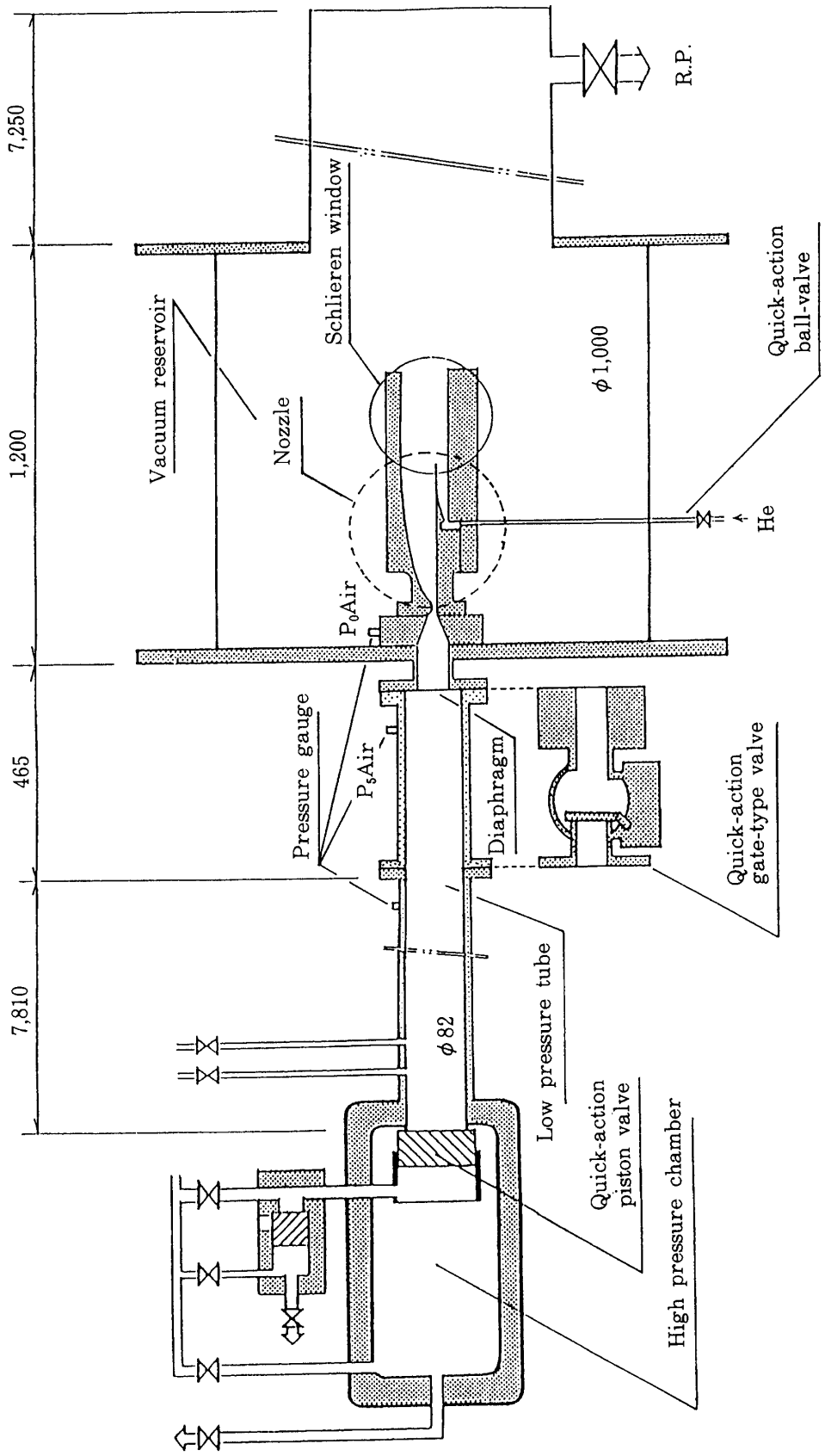

Fig. 2. Experimental set-up.

The nominal condition for the air flow is: 2.93 *kPa* for static pressure, 226 *K* for temperature, 3.4 for Mach number at uniform region of the shock-free nozzle (or at the exit of the wedge type nozzle) and 3.2×10^6 $(1/m)$ for Reynolds number. The nominal condition for helium is: 2.93 *kPa* for static pressure, 43.4 *K* for temperature, 4.2 for Mach number at the uniform region of the shock-free nozzle (or at the exit of the wedge type nozzle) and 1.74×10^7 $(1/m)$ for Reynolds number.

The typical pressure histories for the stagnation condition for air and helium are shown in Fig. 3. The origin of time in Fig. 3a and Fig. 3b is arbitrary. The lower lines in Fig. 3a and 3b show the monitor signals of the fast action-valves just behind the nozzles. Both of the pressure show a sudden rise after opening the valves, and attain constant level. The duration time of the constant pressure is about 2 *msec* for the air flow while the one for the helium flow is long enough. In the light of the air pressure duration, the steady parallel supersonic flows can be expected to be obtained during about 2 *msec* at the present facility. Synchronizing the timings of the generation of the air and of the helium flow, the steady parallel supersonic flows having the duration time of 2 *msec* are attained at the present facility.

3. Flow Visualization and In-site Measurement by Mass Sampling Probe

Schlieren photographies of the flows generated at each Cases are shown in Fig. 4. Papamoschou and Roshko defined the visual growth rate of the mixing layer from the schlieren photography and examined the effect of compressibility on the visual growth rate of the mixing layer.[*3*] However, it is basically rather ambiguous to discern the mixing layer from the photography. To avoid the ambiguity, the in-site measurement of the mixing process is attempted in the present experiment.

The basic idea for the present measurement system is to sample the mixture gas from the region inside the mixing layer and to analyze it by means of a mass-spectrometer. From the measurement we can obtain a concentration ratio of helium at the point where the sampled gas is picked out. A schematic figure of the measurement system is shown in Fig. 5. The measurement system is composed of the probe mounted on the sampling-valve driver which manages the gas sampling process, and the mass spectrometer. The gas entering into the probe is steadily purged to avoid the effect of the gas coming into until the steady mixing layer is attained. When the probe is inserted into the mixing layer, and the gas flow inside the probe becomes steady, the mixture gas inside the probe is sampled through the fast action valve equipped inside the probe and driven by the sampling-valve driver. The tip of the probe is 1*mmø* in diameter. The sampled gas is introduced to the vessel to which the mass spectrometeris attached, and the component of the gas is analyzed by means of the mass spectrometer. The vessel for the sampled gas is evacuated to 0.1 *Pa*

before the sampling and the vessel pressure rises to about 10 *Pa* after the sampling. The purged gas is introduced to the vessel having the volume of 30 *l* which is evacuated to 1.3 *Pa* steadily. The fast action valve inside the probe is driven by an electro-magnetic force supplied by a coil into which an electric current is discharged from a condenser bank, and is driven synchronizing correctly with the steady mixing layer since the valve enables us to sample the gas in around 1*msec*. The condenser bank is charged up to a energy of 400 *J* in a voltage of 400 *V*.

When the mass-sampling probe is inserted to the flow, the probe disturbs the flow. However, as can be seen from Fig. 6, there is no discernible difference in the mixing layer from the one without the probe, at least in the upstream region of the probe tip.

The signal of the mass spectrometer for each species, I_i, is related to the flux of the species through the probe,

$$I_i \propto n_i \upsilon A,$$

where n_i is the number density of the species, υ the velocity and A the area of the hole at the tip of the probe. The concentration ratio of the helium to the air is assumed to be equal to the ratio of helium to oxygen which is one of the components of air. Hence the ratio of the signal intensity of the mass spectrometer between helium and oxygen is related to the concentration ratio between them;

$$n_{H_e}/n_{A_{ir}} = n_{He}/n_{O2} = F\,(I_{He}/I_{O_2}),$$

where the function F can be determined by an appropriate calibration of the measurement system. The typical signal for the mass spectrometer is shown in Fig. 7 where the signal corresponding to helium and oxygen appears alternately according to the control signal from the measurement system.

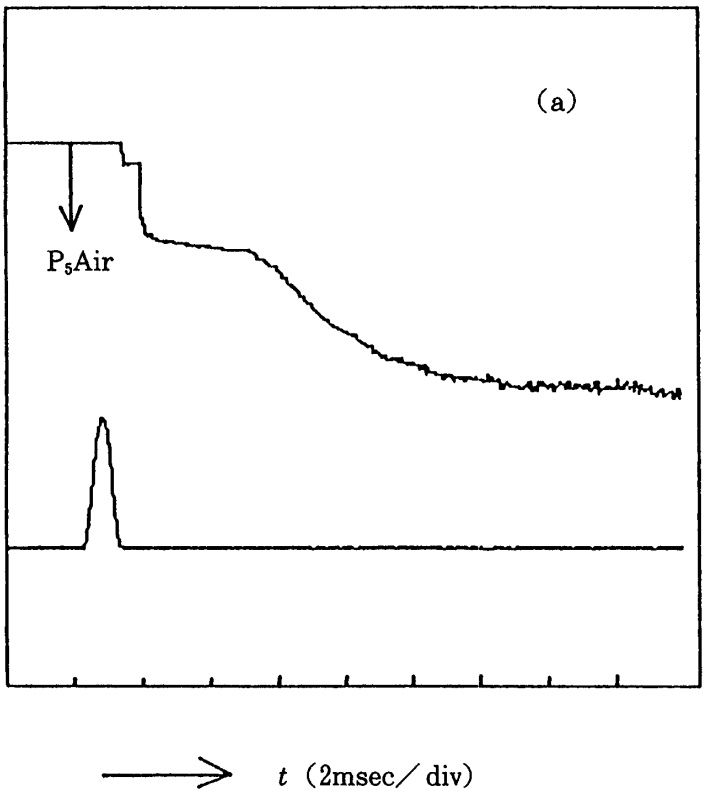

Fig. 3. Temporal pressure variation at the stagnant condition for air (in (a)) and helium (in b)) flows. The origins of time in both figures are arbitrary.

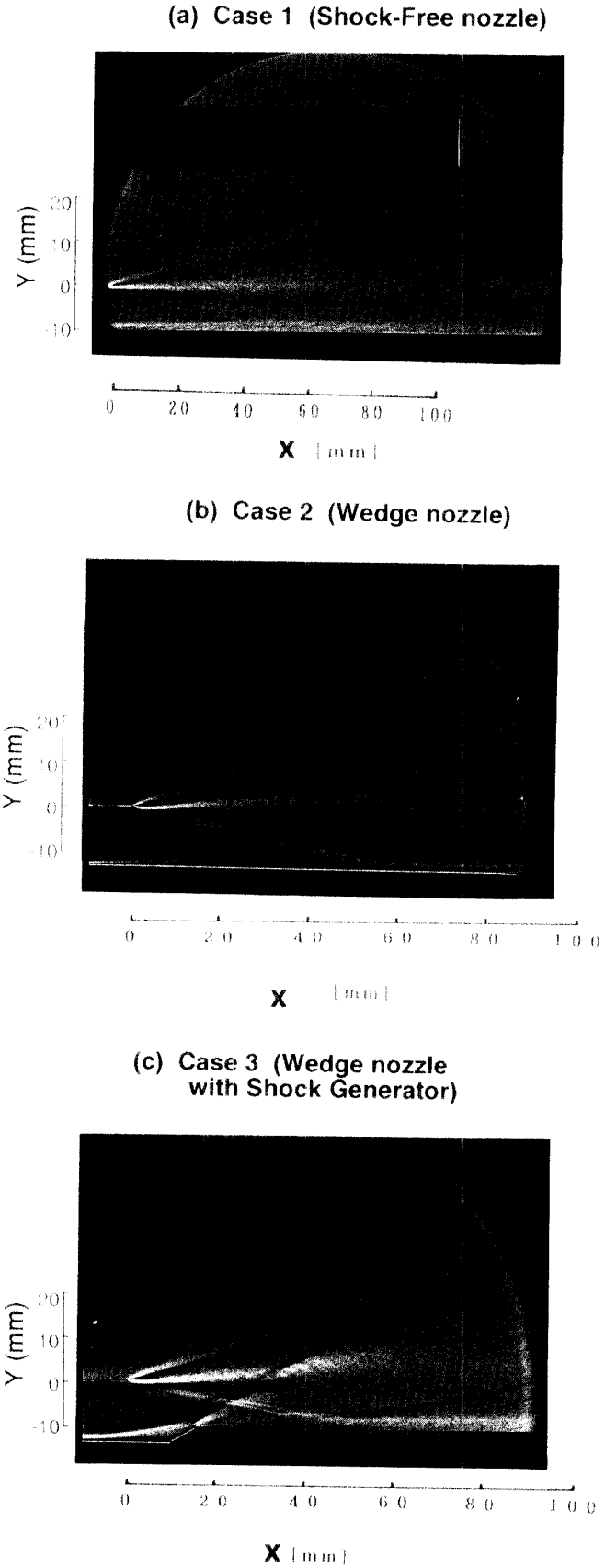

Fig. 4. Schlieren photographies for different nozzle configurations of Case 1 (in (a)), Case 2 (in (b)) and Case 3 (in (c)).

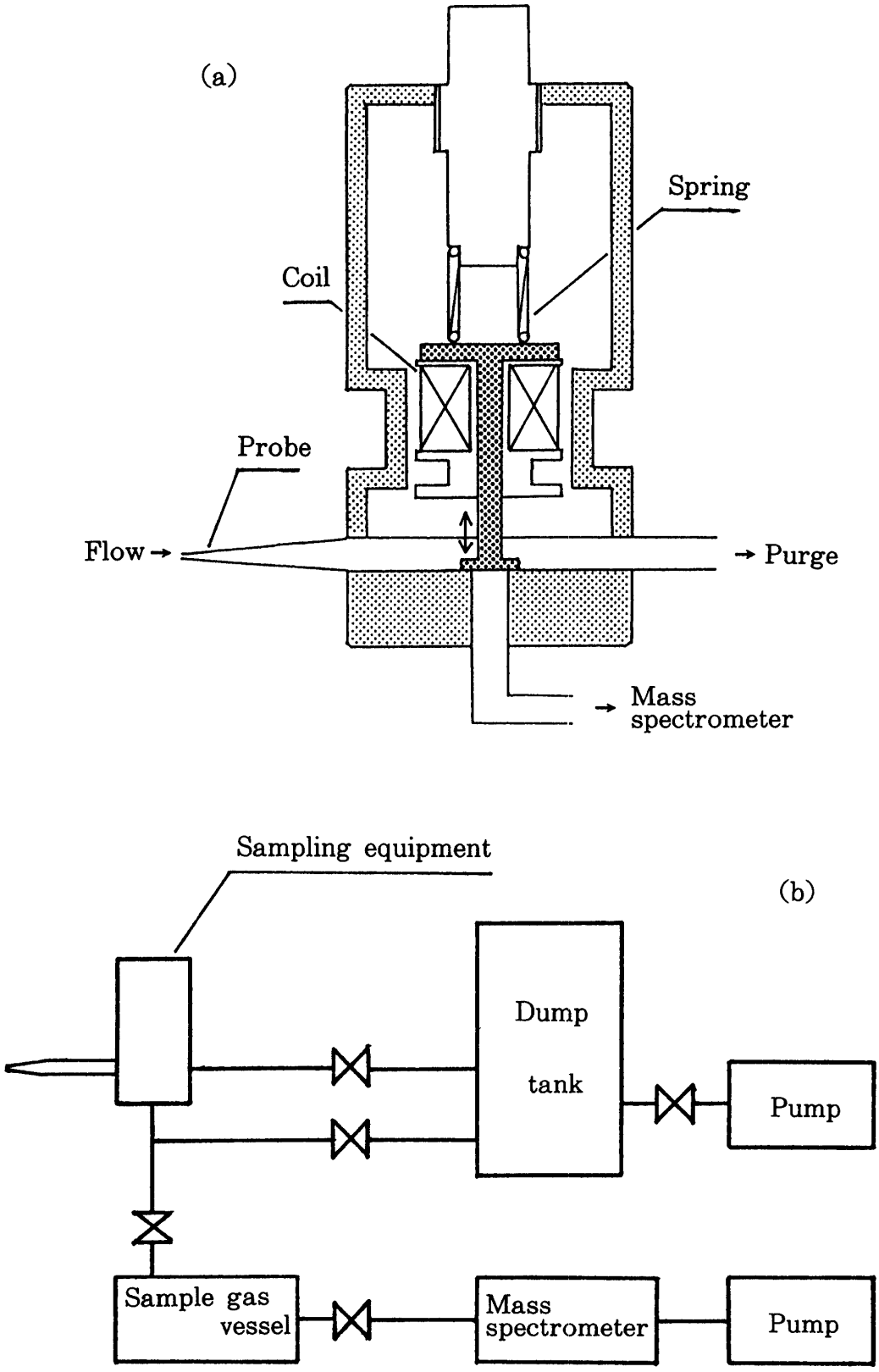

Fig. 5. Schematic figures of the sampling equipment (in (a)) and the probe (in (b)).

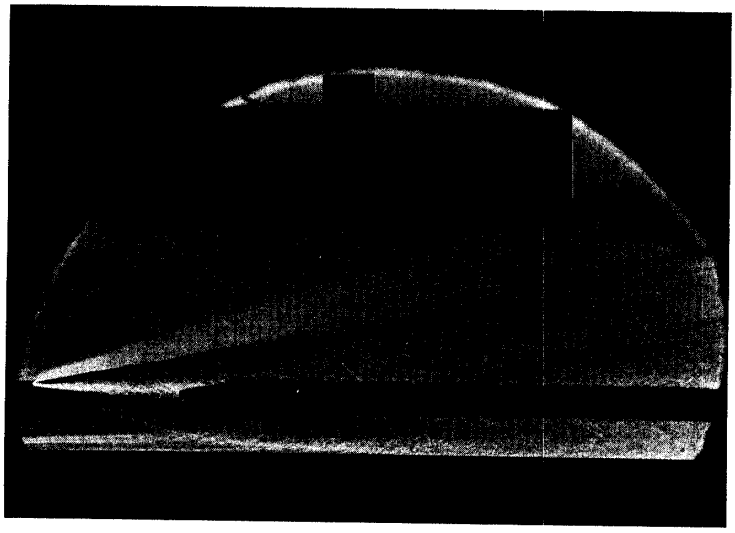

Fig. 6. Schlieren photography of the flow field for the Case 1 when the sampling probe is inserted.

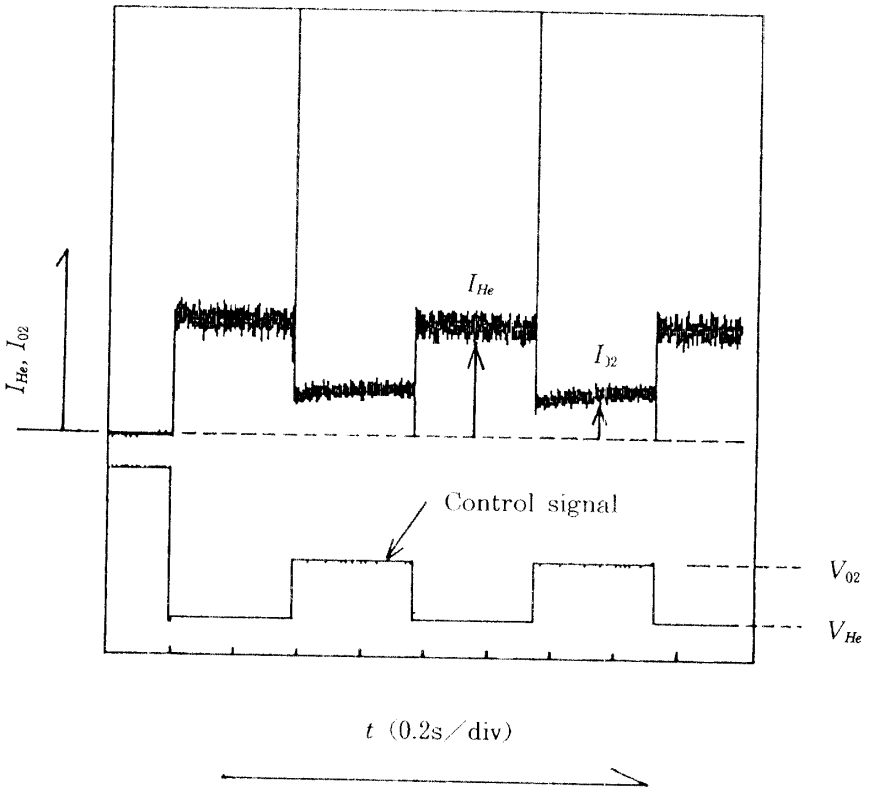

Fig. 7. Typical output from the mass spectrometer.

4. Results

The distributions of the helium concentration ratio inside the mixing layer are shown in Fig. 8. They are measured by means of the present in-site measurement method. The measurements are conducted along perpendicular direction (y-direction) to the flow by 2 mm step at several points along the flow direction (x-direction) by about 5 mm step. Each measurement data is obtained by each operation of the facility. The error bar for the measurement at a fixed point for each operation is negligibly small. This accuracy was achieved by the good reproducibility of the flow which is a most important feature of the present facility. To see the behavior of the growth of the mixing layer, the concentration ratio contour (Fig. 9) is suitable. From the figure it is easy to see that the mixing layer in each case grows along the flow direction. Needless to say, the location of the mixing layer which can be discerned from the Schlieren photography of the flow is almost the same as the one represented by the concentration ratio contour.

Here we define the width of the mixing layer "b" at each location along the stream, as the distance from the location of 10% to that of 90% in the concentration ratio of helium. The mixing layer width increases almost monotonously along the flow direction as shown in Fig. 10. Hence we define the growth rate db/dx of the mixing layer by applying the linear curve-fitting method to the plot of the measured mixing layer width versus the length along the stream direction. The growth rate for each case is tabulated in Table 1. In the table, the growth rate for each case is normalized by the one without compressibility effect [*3*]. Here the growth rate of the mixing layer without the compressibility effect is defined by [*3*],

$$\frac{db_i}{dx} = 0.17\,\frac{(U_1 - U_2)}{U_c}\,, \tag{1}$$

$$U_c = \frac{\sqrt{\rho_1}U_1 + \sqrt{\rho_2}U_2}{\sqrt{\rho_1} + \sqrt{\rho_2}}\,, \tag{2}$$

Table 1. Normalized growth rate of the mixing layer in different configurations.

	Case 1	Case 2	Case 3
In-site Measurement	0.07	0.13	0.16
Visual Growth Rate	0.06	0.11	—

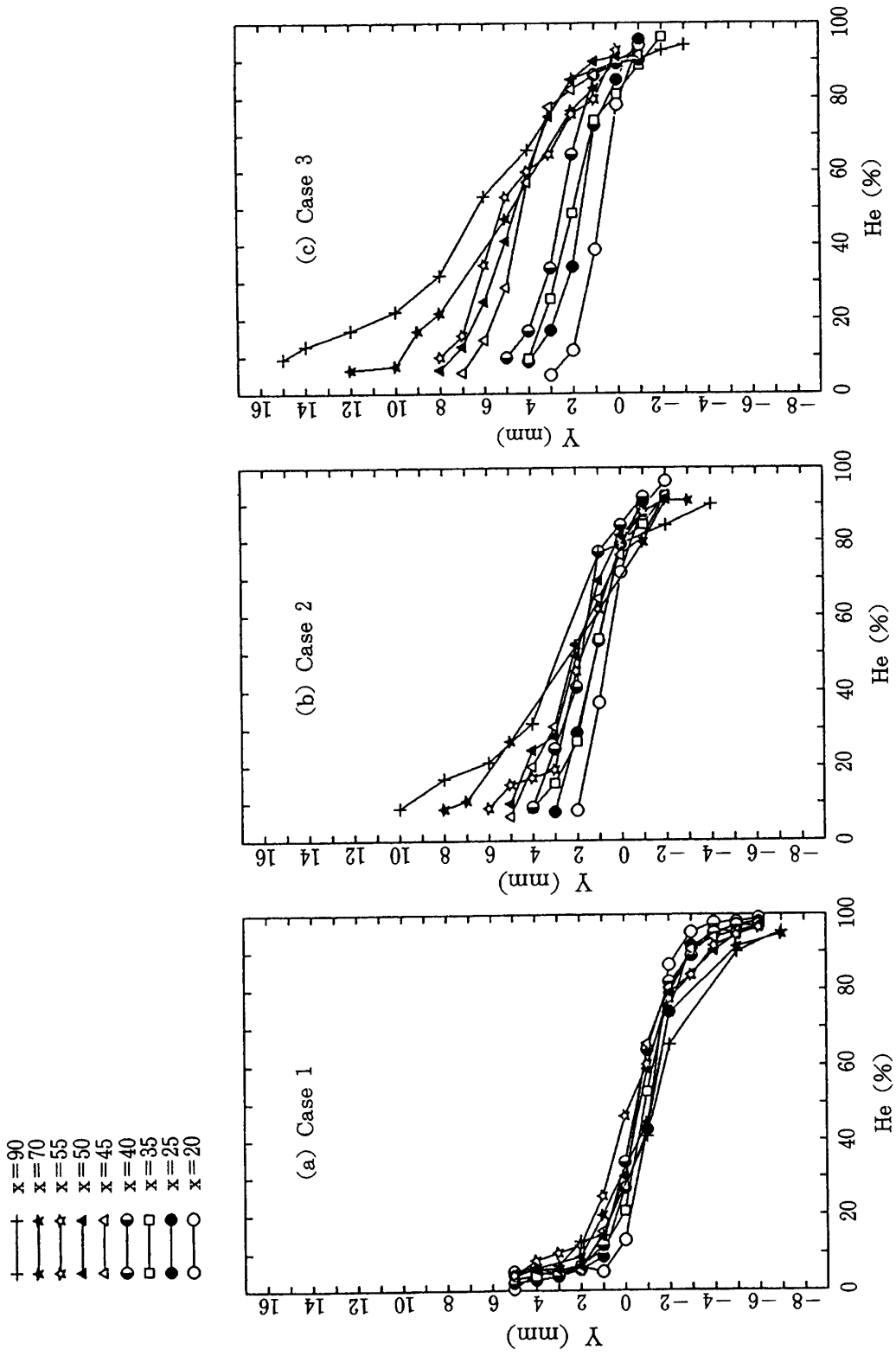

Fig. 8. Concentration ratio distribution along the vertical direction at several points along the flow direction, for Case 1 (in (a)), Case 2 (in (b)) and Case 3 (in (c)).

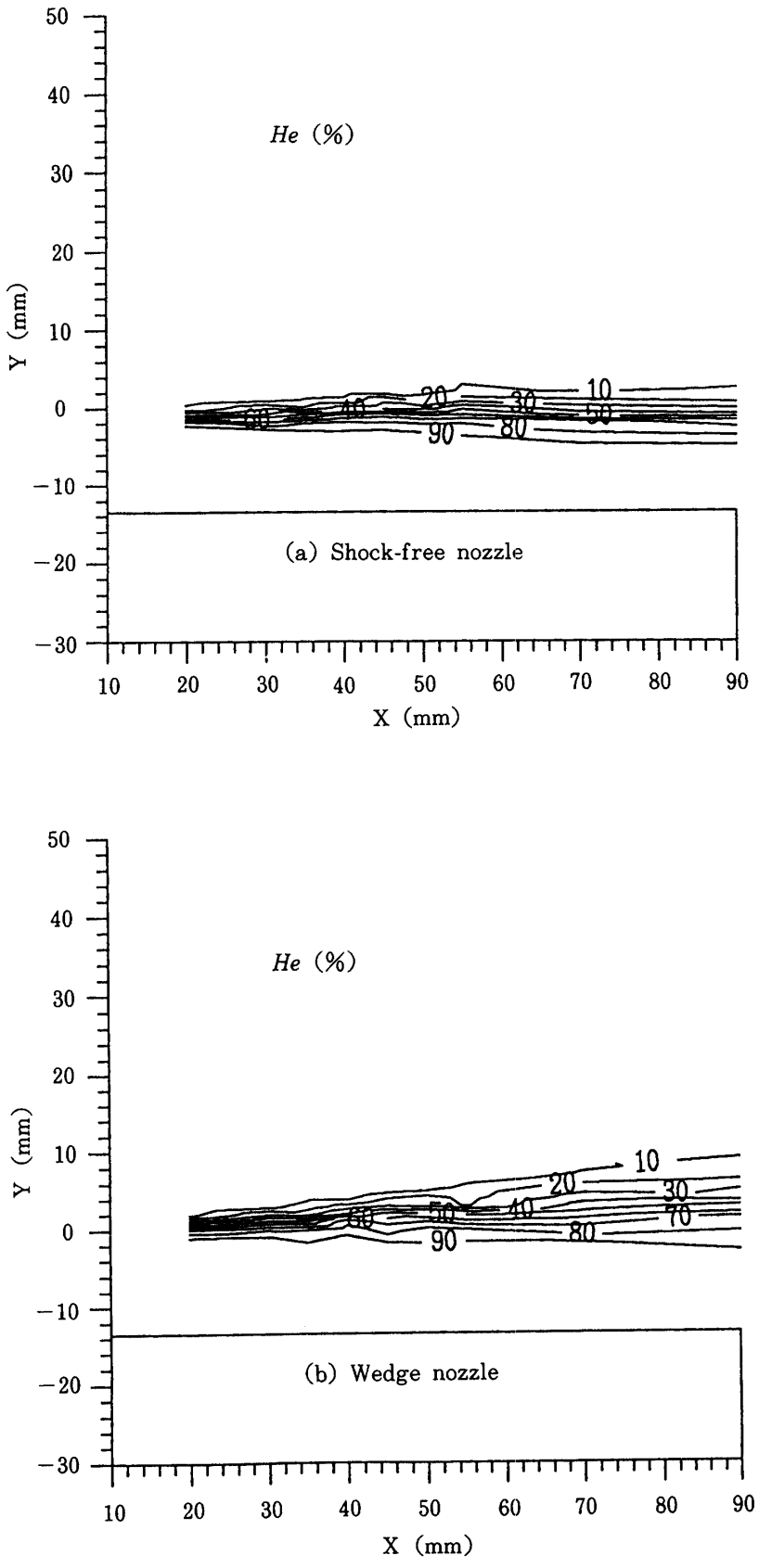

Fig. 9. Contour of concentration ratio of helium for the flow in Case 1 (in (a)), Case 2 (in (b)) and Case 3 (in (c)).

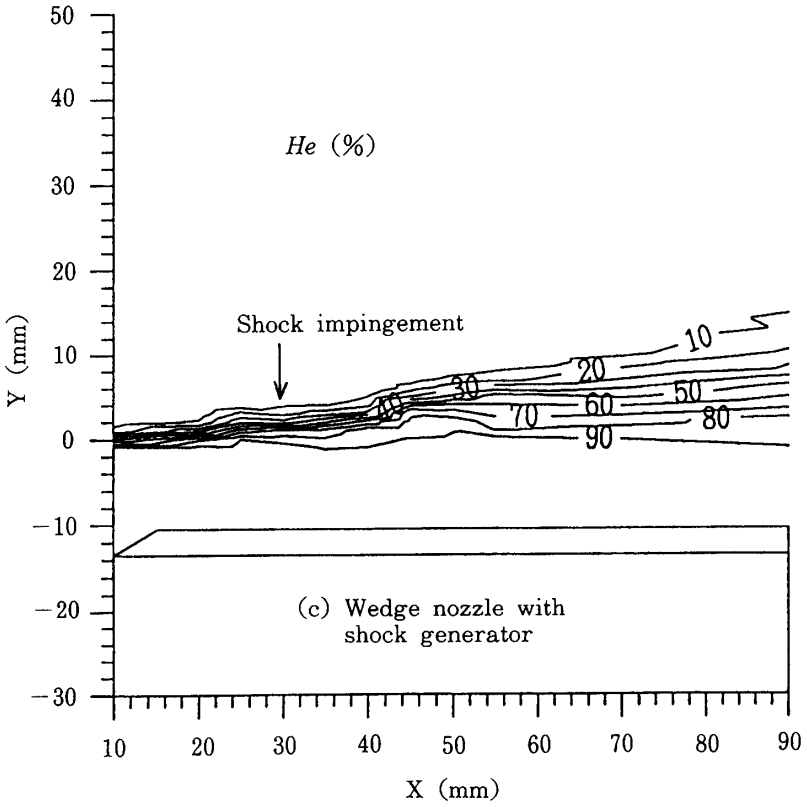

Fig. 9 c

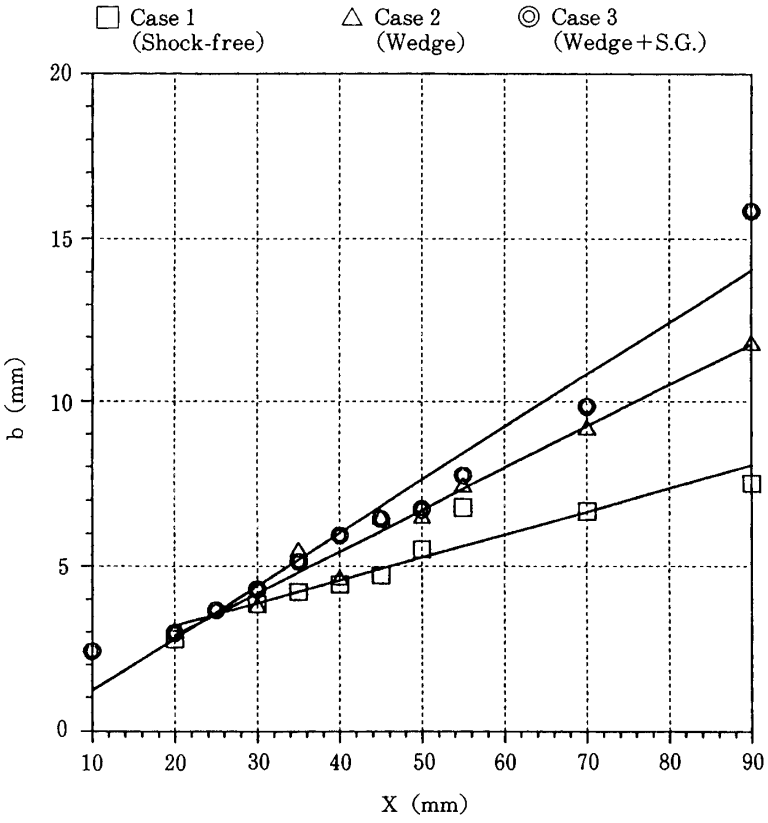

Fig. 10. Variation of mixing layer width along the stream direction (x coordinate).

where U is the flow velocity, ρ the density, and the suffix 1 and 2 stand for values of the high and low speed flow, respectively. In the present experiment, the flow velocity and density for the air flow are 1.0 *km/sec* and $4.5 \times 10^{-2} kg/m^3$, respectively, and those for the helium flow are 1.6 *km/sec* and $3.1 \times 10^{-2} kg/m^3$, respectively. For comparison the normalized visual growth rate is shown at the same table. The visual growth rate was obtained from the Schlieren photography of the flows. The visual growth rate is almost the same as the one obtained from the measurement of the concentration ratio except at the Case 3 where no visual growth rate was obtained because of the difficulty to measure the visual growth rate clearly. The growth rate in Case 2 is about 2 times larger than the one in Case 1 while the growth rate in Case 3 is further larger than the one in Case 2.

The effect of flow compressibility on the visual growth rate is shown in Fig. 11 which is the reproduction of the result by Papamoschou and Roshko [3]. In the figure, the normalized visual growth rate is plotted against the compressibility parameter defined by Gogdanoff [7] as follows;

$$M^+ = \frac{M_1(1 - \lambda_u)}{(1 + \lambda_\rho^{-0.5})\lambda_\gamma^{0.25}},$$

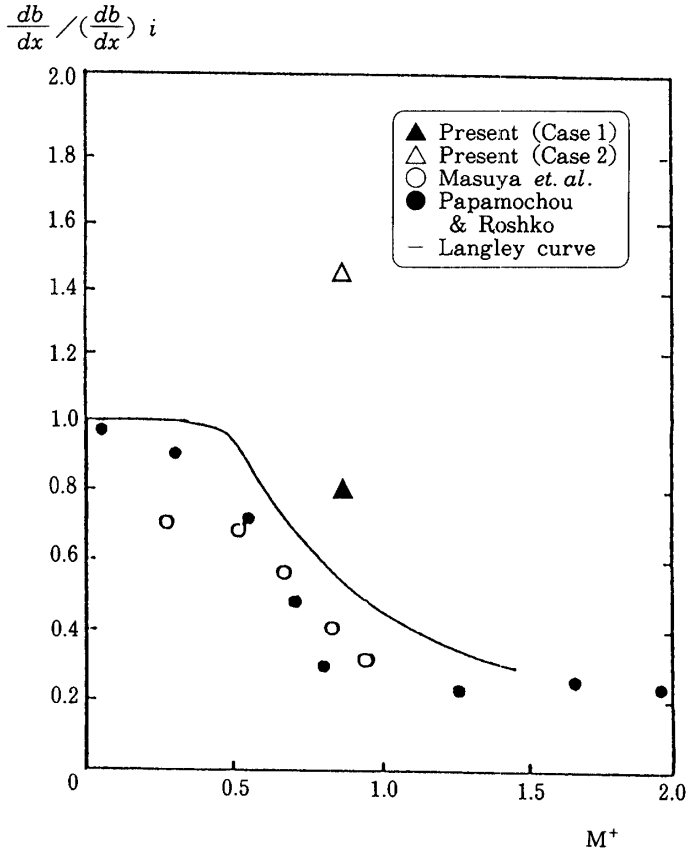

Fig. 11. Normalized growth rate of the mixing layer versus the compressibility factor M^+. The $(db/dx)_i$ is the growth rate without the compressibility effect.

where $\lambda_u = u_2/u_1$, $\lambda_\rho = \rho_2/\rho_1$ and $\lambda_\gamma = \gamma_2/\gamma_1$ [7]. The present results for the growth rate are plotted by ▲ for Case 1, and △ for Case 2, respectively. As expected, the present result for the shock free nozzle almost agrees with the one by Papamoschou and Roshko [3]. The slight difference between them can be attributed to the ambiguity of the measurement of the visual growth rate. Since the growth rate in case 1 can be considered to be the same as the existing value, we can conclude that the effect of steam-wise pressure gradient enhances the growth rate of the mixing layer without the effect, and further, the shock impingement on the mixing layer of Case 2 enhances the growth rate of the mixing layer.

5. Discussions

The present result shows that the growth rate of the mixing layer is affected by the stream-wise pressure gradient, and is enhanced by the effect of the stream-wise pressure gradient in comparison with the one in the shock-free nozzle. The enhancement of the growth rate may be correlated to the vortex generation which is implied by the baroclinic torque appearing in the equation for the vorticity ω;

$$\frac{D\omega_z}{Dt} = -\omega_z\left(\frac{\partial U_x}{\partial x} + \frac{\partial U_y}{\partial y}\right) + \frac{1}{\rho^2}\left(\frac{\partial P}{\partial x}\frac{\partial \rho}{\partial y} - \frac{\partial \rho}{\partial x}\frac{\partial P}{\partial y}\right),$$

where $D\omega_z/Dt$ is a rate of vorticity variation following a fluid element, $\boldsymbol{U}$ the flow velocity, the first term of the right hand side is related to the fluid expansion (or compression) and the second term the baroclinic torque. In the present system of parallel supersonic flows, the significant density gradient exists at the interface since the density of the air flow is different from that of the helium flow. Besides this, in the wedge type nozzle (Case 1), there is a pressure gradient along the flow which is inherent to Mach number changes from 3.4 at the start of the mixing layer to 3.9 at the exit of the nozzle. These gradients normal to each other produces the baroclinic torque of $2.6 \times 10^7 sec^{-2}$ while the typical vorticity of the mixing layer is $1.1 \times 10^5 sec^{-1}$. Since the additional vorticity accelerates the mixing, the vorticity produced by the baroclinic torque is a candidate for the cause of enhancing the growth rate of the mixing layer.

The present result also shows that the shock wave impinging on the mixing layer enhances the growth rate of the mixing layer. When the shock wave impinges and penetrates the mixing layer, its inclination angle changes from the one for the helium flow (about 20 degrees) to the one for the air flow (about 25 degrees) because the Mach number in each supersonic flow is different to each other. This implies that the shock wave must be curved inside

the mixing layer. As known well, this curved shock wave produces the vorticities behind it through the baroclinic torque. In similar to the enhancement by the stream-wise pressure gradient, the enhancement by the shock impingement also may be attributed to the vorticities produced by the curved shock wave through the baroclinic torque.

6. Conclusions

We have examined the flow non-uniformity effect on the mixing layer at the interface between the parallel supersonic flows, by in-site measurement of the concentration ratio inside the mixing layer. As for the flow non-uniformity, a stream-wise pressure gradient and a shock wave impinging on the mixing layer were examined. When a stream-wise pressure gradient exists, the growth rate of the mixing layer is enhanced in comparison to the one without the gradient. As for the cause of the enhancement, the baroclinic torque produced by the stream-wise pressure gradient is a candidate. When the shock wave impinges on the mixing layer, it also enhances the mixing growth rate. The vorticity generation by the curved shock wave penetrating the mixing layer is a candidate for the enhancement of the growth rate of the mixing layer.

Acknowledgment

The authors are grateful to the assistant by Mr. A. Kohama throughout this study.

References

[1] Ferri, A., "Mixing Controlled Supersonic Combustion," *Annual Review of Fluid Mechanics*, Vol. **5**, 1973, pp. 301-338.

[2] Chinzei, N., Masuya, G., Komuro, T., Murakami, A., and Kudo, K., "Spreading of Two-stream Supersonic Turbulent Mixing Layers," *Phys. Fluids*, Vol. **29**, 1986, pp. 1345-1347.

[3] Papamoschou, D. and Roshko, A. "Observations of Supersonic Free Shear Layers," AIAA Paper No. 86-0162, 1986.

[4] Menon, S., "Shock-Wave-Induced Mixing Enhancement in Scramjet Combustors," AIAA Paper No. 89-0104, 1989.

[5] Kumar, A., Bushnell, D.M., and Husani, M.Y., "A Mixing Augmentation Technique for Hypervelocity Scramjets," AIAA Paper No. 87-1882, 1987.

[6] Hatakeyama, M., Funabiki, K. and Abe, T., "An Experimental Study of Supersonic Mixing Process by Using Shock Tunnel Using Quick-Action Valves and Quick-Mass-Sampling Probe Technique," *J. Japan Soc. Aero. Space Sci.*, 1989, pp. 278-284 (in Japanese).

[7] Bogdanoff, D.W., "Compressibility Effects in Turbulent Shear Layers," *AIAA J.* Vol. **21**, 1983, pp. 926-927.